Reinforcing strong coupling with hybrid microcavities for polariton chemistry application

Master's thesis, 23.07.2021

Author:

Hassan Ali Qureshi

Supervisor:

Jussi Toppari
Nemanja Markesevic

UNIVERSITY OF JYVÄSKYLÄ
DEPARTMENT OF PHYSICS

Abstract

The light-matter coupling is a physical phenomenon in which optical modes of light are in resonance with the energy level of matter, thus enabling exchange of energy between them. The strong light-matter coupling is achieved when energy levels of the matter are in resonance with confined light mode and they start exchanging energy in such a way that the rate of this energy exchange overcomes the energy dissipation rate of the system. This usually needs a resonance with a highly confined light mode. The strongly light-matter coupled system acquires new hybrid energy levels that are different from the matter's energy levels. This regime offers a wide range of applications in optoelectronics and chemistry. The strong coupling has made possible the manipulation of chemical reactions without changing the chemical environment of the system, giving rise to a new branch of chemistry known as the polariton chemistry.

This thesis provides comprehensive study on the enhancement of strong coupling by using hybrid cavities made up of two different materials couple to the same confined optical mode. The study includes the absorption evolution of the HBQ molecule system and a hybrid system consisting of HBQ molecule and polycrystalline ZnO. The strong coupling was achieved by depositing molecules inside the Fabry-Pérot cavity. The Rabi split energies of HBQ cavities were 205 meV, 228 meV, and 279 eV whereas, HBQ-ZnO hybrid cavities showed Rabi split energies of 300 meV and 310 meV. The study also includes the effect of strong coupling by changing the cavity geometry. The Rabi split energies in modified geometry were observed as 380 meV, 430 meV, and 490 meV.

Qureshi, Hassan Ali
Outlook and content of Master's Thesis
Master's thesis
Nanoscience Center, University of Jyväskylä, 2021, 49 pages.

Keywords: Strong coupling, polariton chemistry, hybrid microcavities, optical doping, Zinc Oxide, 10-Hydroxybenzo[h]quinoline

Preface

All the praises and gratifications to Almighty and countless blessings to His messenger, peace and blessings upon him, who are the sources of knowledge for entire universe. This manuscript is dedicated to my parents, family and friends for their believe, support and countless prayers. I pay my gratitude to my wife whose continuous support was always with me from the beginning of this degree till day. My gratitude also goes to the Nanoscience Center, JYU for providing me this marvellous opportunity, my supervisors and group-mates for this wonderful, knowledgeable and professional experience.

Jyväskylä 19, July2021

Hassan Ali Qureshi

Contents

1 Introduction

Nature writes its most intimate secrets in light. The light from the sun powers all the life on planet Earth; the light that plants consume to make sugar; the light that is the yardstick of the universe stitching diamonds in the fabric of space and time. It is the same light that defines blackholes when imprisoned and the absence of it prevents us from knowing the nature of dark matter and dark energy. The very nature of light has fascinated humans for centuries. For this reason, optics is known to be one of the oldest known disciplines in science.

Scholars and scientists have been speculating about the nature of light since the era of ancient Greece when they believed that colors are made up of mixtures of lightness and darkness, and layed down the foundations to understand the fundamental nature of light. Just before the start of the second millennium, Ibn Al-Haytham inherited Grecian knowledge and excelled in the field of optics. His 'book of optics' included observations and experiments on light reflection and refraction through lenses and mirrors and provided geometrical arguments on refraction that later became the Snell's law. Further advancements in the field were made; in the 17th century; by Isaac Newton's disquisition that light is made up of streams of particles and his rival Christian Huygens counter thoughts, that light is a spreading wave instead. Luckily or not, both were correct as proven a century later by Thomas Young in his famous double slit experiment and Albert Einstein's photoelectric effect. The advancements of modern science in the early 20th century allowed us to probe deeper to an atomistic level where the formulations of classical physics fail and quantum mechanics emerges that to comprehensively explain the phenomena at atomic and molecular scale.

Before the dawn of quantum mechanics, light and matter were considered as separate entities. However, that began to blur later when quantum mechanics explained the principle of energy exchange in between light and matter. This has led to the exploration of physics and chemistry behind the light-matter coupling, and the attractiveness of hybrid quasi-particle composed of light and matter called as "Polariton".

Cavity quantum electrodynamics (CQED), known to us as the powerhouse of polaritons, is one of the favorite experimental playgrounds for scientists to test, control, and explore quantum objects embedded in confined electromagnetic environments. Thanks to this, recent years have seen blooming of a new field at the junction of CQED and chemistry termed a "Polariton Chemistry". This exciting new field has provided sufficient experimental and theoretical shreds of evidence to harness CQED effects to manipulate chemical properties of material instead of adopting the time consuming synthetic modifications. It was first demonstrated experimentally in 2012 by Hutchison et al. by influencing the reaction rate of Spyropyran derivatives (SPI) through strong light-matter coupling [1].

The light-matter coupling can be categorized into four types depending on the coupling strength: Weak coupling, strong coupling, ultra-strong coupling, and deep strong coupling. The standard model of light-matter coupling can be understood by two coupled harmonic oscillators that can exchange energy. In that scenario, the system can not be explained only by the individual frequencies of the oscillator but the exchange process involved in coupling also needed to be consider. Subsequently, the energy spectrum of the system is modified and sometimes even new frequencies are obtained that depends on the strength of coupling [2].

The regular absorption and emission, which is the working principle of most of the optical devices that surrounds us, happens via weak light-matter interaction. In this regime, the coherent energy transfer between light and matter is not possible as dissipative losses overtakes the coupling strength between the light modes and excitations in matter, thus, merely affecting the radiative decay rate of material. Such a process can also be seen in the so-called Purcell effect [3] where the quantum yield of emission can be enhanced by a resonant electromagnetic field.

Contrarily, in the strong coupling limit [4], the coupling strength between the molecular excitations and confined light modes exceeds dissipative losses of the system that allows the coherent energy transfer between light and matter. This give rise to the aforementioned hybrid quasiparticles known as a Polariton, where the light and matter cannot be considered as separate entities anymore. These strongly coupled light-matter modes are not restricted to the electronic excitations only. A strongly coupled system will be characterized with new eigenstates giving rise to new optical properties different from individual light and matter systems [5].

The ultrastrong coupling was initially predicted by Khurgin in 2001 [6] and

observed in 2005 by Ciuti et al. [7]. It goes beyond weak and strong coupling to reach the coupling strengths comparable to the natural frequencies of the system. This exciting new field is qualitatively different from the strong coupling and enables the observation of unique phenomena, for instance, the generation of entangled photon pair from polariton vacuum [8] and superradiant phase transitions [9]. It has been observed in superconducting circuit systems [10] and multiple quantum wells [11]. In the deep strong coupling regime, the coupling strength exceeds the resonance energy and driving frequency of the system, fundamentally changing its properties. In this ultimate limit of light-matter coupling, the light and matter are expected to decouple and photon starts to self interact with each other. Nevertheless, this regime is novel and absolute understanding is yet to be discovered [12].

The first theoretical studies of hybrid states of light and matter were published by Hopfield in 1958 [13]. Edwin Jaynes and Fred Cummings presented standard model for strong coupling in 1963, now a days well known as Jaynes-Cummings Model [14]. The term polariton was first adopted by Yakovlev et al. in 1975 [15]. The atomic cavity polaritons were first observed in the 1980s by Meschede et al. [16] and demonstration of strong coupling in planar microcavity, with a Rabi split of 2 meV at the temperatures up to 77 K, was first reported by Weisbuch et al. in the 1990s [17]. Agranovich made significant progress in 1997 [18] by providing theoretical evidence of strong coupling in organic and inorganic quantum wells that was proven a year later by Lidzey et al. Lidzey and his coworkers fabricated microcavities embedded with organic crystals, which showed Rabi splitting of 160 meV at room temperature [19]. The demonstration of strong coupling at room temperature proved to be the key development and sparked ever-expanding interest in the field. The idea of optical doping to enhance the strong coupling came from Lidzey et al. in 2004, when they demonstrated the hybrid polaritons consisting of two different layers of molecular J-aggregates leading to the so-called ‘hybrid polaritonic modes [20]. In 2014, Slootsky et al. reported the organic-inorganic hybrid microcavities consisting of 1,4,5,8-Naphthalenetetracarboxylic dianhydride (NTCDA) and Zinc Oxide (ZnO) [21]. These microcavities showed the Rabi splitting of 322 meV in comparison to the 224 meV and 218 meV Rabi splittings for NTCDA and ZnO [21].

In the following thesis, it will be demonstrated that enhancement of strong coupling in different types of excitons on a single light mode is possible. This will be done by utilizing 10-hydroxybenzo[h]quoline (HBQ) molecule and ZnO thin films

in the optical cavity system. The cavity parameters, molecule concentration, and fabrication process will be optimized to study the effect on strong coupling. The structure of the thesis is as follows: In section 2, the basic concepts and theoretical description of light-matter interaction will be introduced. Section 3 will provide details about the experimental method and materials that were used to fabricate and quantify the properties of the optical cavities. Lastly, section 4 will summarize the findings and scope of the studies.

2 Theoretical backgrounds

The light matter interaction happens all the time in our daily life from photosynthesis to watching objects and colors through our eyes. The following chapter will provide an understanding of light and matter interaction at different capacities. The first part will provide the concepts related to the interaction of light with molecules followed by the second section that will provide the details about the optical system and movement of light in different mediums. Finally, the strong coupling will be elaborated with the help of various models.

2.1 Interaction of matter with electromagnetic field

Before going into this section, it is important to know the nature of light. Light, as a wave, is electromagnetic radiation consisting of a synchronized electric and magnetic field propagating through space. The wave nature of light can be described with the famous Maxwell equations. Light is classified into various regions depending on the frequency and wavelength e.g, the visible region of light lays between wavelengths of 400 to 700 nm. Light can also be seen in the form of discrete packets of energy known as 'Quanta' that refers to the particle nature of light [22]. The energy of quanta or photons is related to frequency through the equation (1):

$$E = \hbar\omega, \tag{1}$$

where $\hbar$ is the Planck's constant and ω is the angular frequency of light. The interaction of photon with a molecule leads to the absorption of photon and changing the molecule's ground state to excited state. Upon de-excitation, that results in various radiative and non-radiative processes.

2.1.1 Molecular absorption

Molecular absorption can be defined as a process in which a molecule is excited from ground state to excited state after interacting with light of certain wavelength. Each electronic transition is associated with number of vibrational and rotational transitions with much smaller energies. The majority of molecules occupy the lowest vibrational level of ground state at room temperature are moved to excited state upon interaction with light. The Boltzmann distribution given in equation (2) is used to describe the population of molecules in the $j-th$ vibrational level at given temperature [23]:

$$\frac{N_j}{N_o} = \exp -\frac{E_j - E_o}{k_B T}. \tag{2}$$

The above equation (2) implies that molecules always have some vibrational excitations. However, at the room temperature all the molecules can easily be at electrical ground state, since the energies of the electrical excitations (>1 eV) are usually much higher than the thermal energy of the room temperature which is about 0.026 eV. Vibrational excitations are at this same meV energy region and can be even smaller, thus they are thermally excited along the equation (2).

The energy gap ΔE between the molecular orbitals defines the wavelengths at which the molecule absorbs light. The gap depends on the structure of the molecule whereas absorption in particular spectral region depends on the particular group of atoms. For instance, overlapping of two adjacent p-orbitals forms conjugated π-systems that decreases the energy gap between the highest occupied molecular orbitals and the lowest occupied molecular orbitals of a particular molecule that eventually leads to the absorption of lower energy photon. An example of molecular electronic excitations are shown in Figure 3. The σ, π or n refers to occupied valence orbitals from which an electron can make transition after absorbing a photon into unoccupied antibonding orbital σ^* or π^*.

Figure 1. Energy levels for possible electronic transitions.

2.1.2 Transition dipole moment

The transition dipole moment is the transition induced to a molecule or atom due to oscillating electric field component of the radiation. An atoms or a molecule is composed of positive nuclei and negatively charged electrons that interacts with the electromagnetic field. This interaction causes the transition that can be seen in absorption and emission spectroscopies. In general, the transition dipole is a complex vector quantity that contains phase factors associated with two states. The transition dipole moment between an initial and final state is defined as

$$\langle \psi_f | \, \hat{\mu} \, | \psi_i \rangle = \int \psi_f^* \hat{\mu} \psi_i d^3 \vec{r}, \tag{3}$$

where ψ_i and ψ_f are the initial and final state and $\hat{\mu}$ is the electric dipole moment operator defined as

$$\hat{\mu} = \sum_{\alpha} \vec{q}_\alpha \vec{r}_\alpha, \tag{4}$$

where $\vec{q}_\alpha$ and $\vec{r}_\alpha$ are the charge and position vectors of a point charge α. The probability for the transition to occur is given by

$$P \propto \left| \int \psi_f^* \hat{\mu} \psi_i d^3 \vec{r} \right|^2. \tag{5}$$

It implies that for interaction, dipole must be oscillating at the same frequency with electromagnetic field.

2.2 Dynamics of Optical Systems

2.2.1 Fresnel equations

The interaction of electromagnetic wave with a medium an interface between two materials can lead to reflection, refraction and transmission. Fresnel equations are the set of equations that describes the relation between the electric fields of transmitted and reflected waves to the electric field of incident wave for both s and p polarizations. The Fresnel's coefficients for reflection, r_s, and transmission, t_s, for s- and p-polarized light are given by [24]

$$r_s = \frac{n_1 \cos\theta_i - n_2 \cos\theta_t}{n_1 \cos\theta_i + n_2 \cos\theta_t}, \tag{6}$$

$$t_s = \frac{2n_1 \cos\theta_i}{n_1 \cos\theta_i + n_2 \cos\theta_t}, \tag{7}$$

$$r_p = \frac{n_2 \cos\theta_i - n_1 \cos\theta_t}{n_1 \cos\theta_i + n_2 \cos\theta_t}, \tag{8}$$

$$t_p = \frac{2n_1 \cos\theta_i}{n_2 \cos\theta_i + n_1 \cos\theta_t}. \tag{9}$$

Where θ_i is the angle of incidence, θ_t is the transmission angle and n_1, n_2 are the reflective indices of the material 1 and 2 as shown in Figure 2.

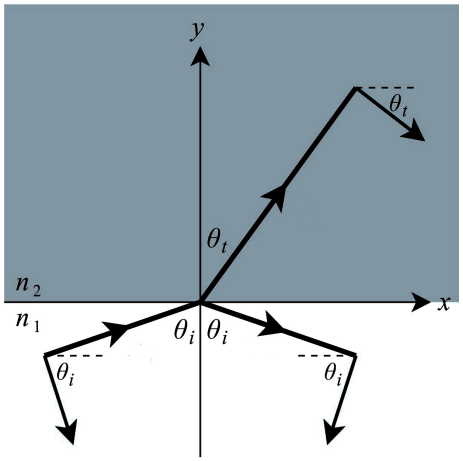

Figure 2. Incident, reflected and transmitted waves from a medium with refractive index n_1 to a medium with refractive index n_2.

2.2.2 Transfer matrix method (TMM)

The reflection of light between two media is described by Fresnel equations. However, light propagation through a multilayered system is challenging to model with conventional geometric series mathematics accounting for all the reflections, transmissions, and summing up the total reflected wave. A rather simple approach known as Transfer Matrix Method (TMM), derived by Herbecke [25], is widely used in optics to analyze the propagation of electromagnetic waves through a layered system. The fundamental of TMM is that, according to Maxwell's equation, there are boundary conditions for electromagnetic waves between different mediums with different reflective indices and if the field is known at the beginning of layer, it can be calculated at the end of other layer with simple matrix operation utilizing the boundary conditions. The method involves stacking of individual layer matrices to form a system matrix and converting this system matrix into transmission and reflection coefficients.

Instead of going into detail, we will formulate the generalized form of TMM. Let us assume the electromagnetic wave is propagating through layered system at normal incident along z-axis. The electric field within one layer can be represented as the superposition of forward and backward propagating plane waves corresponds to transmitted and reflected waves. Mathematically:

$$\vec{E}(z) = A_R e^{i\vec{k}\cdot\vec{z}} + A_L e^{-i\vec{k}\cdot\vec{z}}, \tag{10}$$

where A_R and A_L are the amplitudes and $\vec{k}$ is the wave vector for the forward and backward moving waves respectively. The transfer matrix M_n that relates E_z at the beginning and end of this layer must then perform a transform:

$$M_n \begin{pmatrix} A_R + A_L \\ (k/k_o)(A_R + A_L) \end{pmatrix} = \begin{pmatrix} A_R e^{ika} + A_L e^{-ika} \\ (k/k_o)(A_R e^{ika} - A_L e^{-ika}) \end{pmatrix}, \tag{11}$$

where a corresponds to thickness of the material. Matrix M_n of equation (9) will be

$$M_n = \begin{pmatrix} \cos(ka) & i\sin(ka)/(k/k_o) \\ i(k/k_o)\sin(ka) & \cos(ka) \end{pmatrix}. \tag{12}$$

The system transfer matrix M_s is thus, the matrix product of all individual transfer

matrices M_n

$$M_s = M_1.M_2.M_3...M_n. \tag{13}$$

2.2.3 Optical resonators

Optical resonators or optical cavities are the structures that can confine light at the certain resonance frequencies. A Fabry-Pérot cavity, named after Charles Fabry and Alfred Pérot, is the simplest design of an optical resonator consisting of two parallel plane mirrors separated by dielectric medium, where the light is trapped and reflected back and forth between the mirrors. A schematic representation of such a cavity is shown in Figure 3.

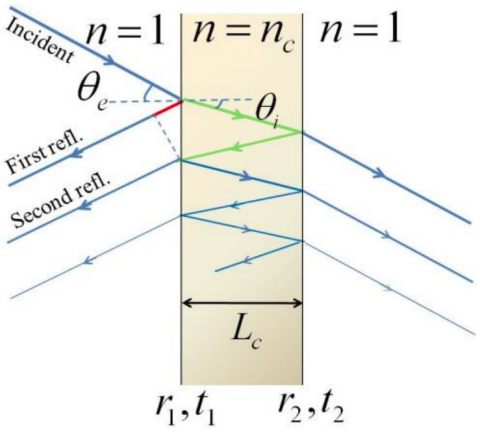

Figure 3. Schematic picture of Fabry-Pérot structure. [26]

A typical Fabry-Pérot cavity works in a way that a light is projected on a cavity. A small portion of light is reflected back from first mirror while the rest is transmitted. The transmitted portion then falls on second mirror and a part of light is again leaked from the second mirror while the rest is reflected back and head towards the first mirror and same phenomena happens again many times in the cavity. As there are many light waves bouncing back and forth inside the cavity, they will interfere. The constructive interference will lead to amplification and create standing waves with resonant mode inside the cavity while the destructive interference will eventually lead to the destruction of such wavelengths. The resonant condition is given by

$$L_{cav} = \frac{m\lambda}{2n}, \tag{14}$$

where λ is the wavelength and and n reflective index of the dielectric inside the cavity.

The equation (14) indicates that the distance between two mirrors L_{cav} should be integer multiple m of half of the intracavity wavelengths λ.

Confinement of light within optical cavities are quantified by mode volume V_{eff} and quality factor Q [27]. The effective mode volume is given as [28, 29]

$$V_{eff} = \frac{\int \epsilon(\vec{r})|\vec{E}(\vec{r})|^2 d^3r}{max(\vec{E}(\vec{r}|\vec{E}(\vec{r}|^2)}, \tag{15}$$

where $\vec{E}(\vec{r})$ is the electric field position at the position $\vec{r}$ and $\epsilon(\vec{r})$ is the dielectric function. The quality factor determines the number of reflections of the photon before it leaves the cavity. Thus the quality factor is defined as

$$Q = 2\pi \frac{E_{stored}}{E_{dissipated}}. \tag{16}$$

The above equation describes ratio of stored energy to the energy lost per cycle. Measuring the stored and dissipated energy is strenuous task, thus, there is another way to describe quality factor that can be easily determined with simple spectroscopic measurement. The equation is given as

$$Q = \frac{\omega_o}{\sigma}, \tag{17}$$

where σ is the spectral width that describes loss and ω_o is the resonance frequency. One can tune the layer thickness and material by using TMM and Fresnel's coefficients to produce highly absorptive cavities at desired wavelengths.

2.2.4 Cavity dispersion

In the TMM, we have seen that the transfer matrix depends on the z-component of the wavevector, $\vec{k}$, used in equation (10) depends on the angle of incidence θ_n by following relation.

$$k_z = k_o \cos\theta_n. \tag{18}$$

It is evident from the above equation that transmission, absorption and reflection have angular dispersion. This effect arises due to the change in wave's phase vector in the cavity. The resonance of the cavity moves to higher energies with changes in

incident angle. The energy of optical cavity is given by

$$E_c = \frac{\hbar c}{n_c}\sqrt{(\frac{m\lambda}{L_{cav}})^2 + (\frac{2\pi}{\lambda}\sin\theta_n)^2}, \tag{19}$$

where n_c is the reflective index of the medium surrounding the cavity.

The potential benefit of dispersive cavity is the tunability. One can use TMM to design the cavity with absorption maximum according to the requirement. Fabrication, however, is a tedious job as the cavity layer thicknesses needed to be precise up to nanometer scale. Nevertheless, small fabrication imperfections can still be covered by tuning the incident angle.

2.3 Strong Coupling Theory

Strong coupling has been described with various theoretical models including classical, semi classical and quantum mechanical model and this section will explain each model in detail. However, the specifications of each model is different i.e. Classical model provides easy and quick analysis of strong coupling, the semi-classical model gives adequate physical insight of the coupling mechanism while the quantum model provides the most precise and detailed explanation. The selection of the models depends on the nature of application and requirements.

2.3.1 Classical model

In the classical model [30], the strong coupling is described as atom/molecule dipole transitions coupled to an optical field expressed as simple harmonic oscillators [2]. Let's assume two harmonic oscillators having masses m_1 and m_2, spring constant k_1 and k_2 and frequency ω_1 and ω_2 respectively, as shown in Figure 4.

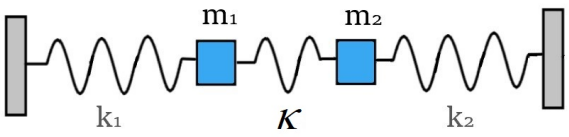

Figure 4. Strong coupling regime illustrated by classical harmonic oscillators. The coupling κ leads to change in eigenfrequencies that leads to characteristic frequency splitting

In the absence of coupling κ=0, the eigenfrequencies of oscillators will be $\omega_1^\circ = \sqrt{\frac{k_1}{m_1}}$ and $\omega_2^\circ = \sqrt{\frac{k_2}{m_2}}$. If the two harmonic oscillators are coupled together with the spring of constant κ ($\kappa \neq 0$), the equations of motions will become

$$m_1\ddot{x}_1 + k_1x_1 + \kappa(x_1 - x_2) = 0, \tag{20}$$

$$m_2\ddot{x}_2 + k_2x_2 - \kappa(x_1 - x_2) = 0, \tag{21}$$

we insert solution of form $x_i(t) = x_i^\circ e^{-i\omega_\pm t}$ in equations (20) and (21) to obtain two coupled linear equations for x_1° and x_2° given below

$$-m_1\omega_\pm^2 x_1^\circ + k_1x_1^\circ + \kappa(x_1^\circ - x_2^\circ) = 0, \tag{22}$$

$$-m_2\omega_\pm^2 x_2^\circ + k_2x_2^\circ - \kappa(x_1^\circ - x_2^\circ) = 0. \tag{23}$$

The equations (22) and (23) can be written in matrix form as

$$\begin{bmatrix} -m_1\omega_\pm^2 + k_1 + \kappa & -\kappa \\ -\kappa & -m_2\omega_\pm^2 + k_2 + \kappa \end{bmatrix} \begin{bmatrix} x_1^\circ \\ x_2^\circ \end{bmatrix} = 0,$$

non-trivial solutions of these equations only exist if the determinant of above matrix is equal to zero. After solving, the resulting characteristic equation yields

$$\omega_\pm^2 = \frac{1}{2}[(\omega_1^2 + \omega_2^2) \pm \sqrt{(\omega_1^2 - \omega_2^2)^2 + 4\Omega^2\omega_1\omega_2}], \tag{24}$$

where $\omega_1 = \sqrt{\frac{k_1+\kappa}{m_1}}$, $\omega_2 = \sqrt{\frac{k_2+\kappa}{m_2}}$ and the term $\Omega = \sqrt{\frac{\kappa^2 m_1 m_2}{\omega_1\omega_2}}$ is the splitting frequency. We will set the values $k_1 = k_\circ$, $k_2 = k_\circ + \Delta k$ and $m_1 = m_2 = 0$ to illustrate the solutions given in equation (24). Figure 5(a) shows the frequencies of two oscillators when the coupling $\kappa = 0$. If the Δk is increased from $-k_\circ$ to $k_\circ$, the frequency of k_1 will remain constant, while the frequency of k_2 will increase to $\sqrt{2}\omega_\circ$. After the coupling is introduced, the two curves shown in Figure 5(b), will no longer intersect with each other and the characteristic anti-crossing behaviour will appear which is the fingerprint of strong coupling. The splitting frequency Ω is directly proportional to coupling κ, therefore the anti-crossing behaviour will increase with increasing coupling strength.

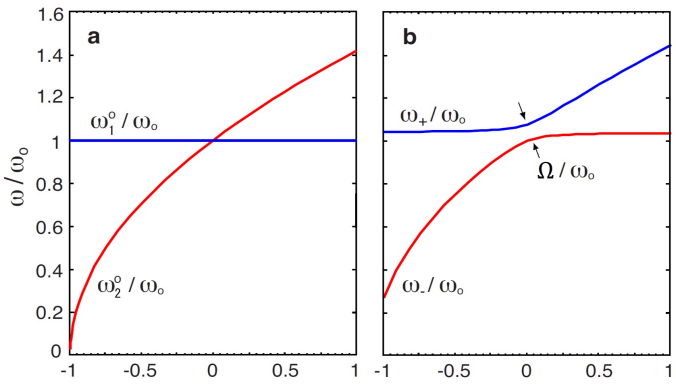

Figure 5. The frequencies of two oscillators when (a) uncoupled state $\kappa = 0$, (b) coupled state $\kappa \neq 0$ where $\Omega = [\omega_+ - \omega_-]$.

Note that we ignored the damping during our analysis for the convenience. However it should be kept in mind that the damping or energy dissipation should be smaller than coupling strength in order to observe strong coupling.

2.3.2 Semi-classical model

In the semi-classical model [2], the excitons are treated as two level system with a ground state $|g\rangle$ (could be any electronic level and not just ground state) and excited state $|e\rangle$, while electromagnetic field remains classical that can be described by $\vec{E}cos(\omega,t)e^{i\vec{k}\cdot\vec{r}}$ where, ω represents the frequency and $\vec{k}$ represents the wave vector of the cavity mode. $\vec{E}$ contains the amplitude and polarization vector of the field. The damping is not included here in order to have the well defined mode with narrow frequency. We consider here a simple plane wave $e^{i\vec{k}\cdot\vec{r}}$ [31], vector basis $|g\rangle = \left(\begin{smallmatrix}0\\1\end{smallmatrix}\right)$ for ground state and $|e\rangle = \left(\begin{smallmatrix}1\\0\end{smallmatrix}\right)$ for excited state. $\hat{\sigma_+} = \left(\begin{smallmatrix}0&1\\0&0\end{smallmatrix}\right)$ represents transition from the ground state to the excited state and the inverse process in defined by $\hat{\sigma_-}$ $= \left(\begin{smallmatrix}0&0\\1&0\end{smallmatrix}\right)$, while the energies of the system can be expressed with $\hat{\sigma_z} = \left(\begin{smallmatrix}1&0\\0&-1\end{smallmatrix}\right)$ and identity matrix $\hat{\mathrm{I}} = \left(\begin{smallmatrix}1&0\\0&1\end{smallmatrix}\right)$. The Hamiltonian of system consisting of a single quantum emitter and the electromagnetic field can be defined as

$$\hat{\mathrm{H}} = \frac{1}{2}E_e(\hat{\mathrm{I}} + \hat{\sigma_z}) + \frac{1}{2}E_g(\hat{\mathrm{I}} - \hat{\sigma_z}) + \hbar\Omega_r(\hat{\sigma_+} + \hat{\sigma_-})\cos(\omega t), \tag{25}$$

where, Ω_r is the semi-classical Rabi frequency that is proportional to the dipole moment times the field amplitude. The derivation of this Hamiltonian is described briefly in the chapter 2 of [32]. Then we will apply the Rotating Wave Approximation (RWA). The RWA accounts for neglecting fast oscillating time dependencies because

the fast oscillating time terms contribute less to the two level system dynamics. Thus, RWA makes it easier to observe the smaller frequencies that describes the dynamics of system by neglecting the rapidly oscillating terms. The transformed Hamiltonian after applying RWA is given as

$$\hat{\mathrm{H}} = -\frac{\hbar\delta}{2}\hat{\sigma_z} + \frac{\hbar\Omega_r}{2}(\hat{\sigma_+} + \hat{\sigma_-}), \tag{26}$$

here, $\delta = \omega - \omega_\circ$ are the detuning frequencies which from the resonance are at, $\omega = \omega_\circ$. The equation (26) forms 2×2 matrix Hamiltonian that will give the eigen values of the system as

$$E_{1,2} = \pm\frac{1}{2}\hbar\sqrt{\delta^2 + \Omega_r^2}, \tag{27}$$

where $\sqrt{\delta^2 + \Omega_r^2} = \Omega$ is the so called generalized Rabi frequency. If the system is in resonance i.e, $\delta = 0$. Then one has energy

$$E_{1,2} = \pm\frac{\hbar\Omega_r}{2}, \tag{28}$$

and expressions for upper and lower polaritons are

$$|2\rangle = \frac{1}{\sqrt{2}}[|e\rangle + |g\rangle], \tag{29}$$

$$|1\rangle = \frac{1}{\sqrt{2}}[-|e\rangle + |g\rangle]. \tag{30}$$

The equations (29) and (30) implies that the eigenstates of the system are in equivalent superposition between ground and excited state.

2.3.3 Quantum model

The quantum mechanical model of strong coupling [33, 34] can be described by a simple two level energy system and a quantized field. The energies of this two level system and quantized electromagnetic field within the rotating wave approximation is defined by a Jaynes-Cumming Hamiltonian[14]

$$\hat{\mathrm{H}_{\mathrm{JC}}} = -\frac{1}{2}\hbar\omega_\circ\hat{\sigma_z} + \hbar\omega\hat{a}^\dagger\hat{a} - i\frac{\hbar\Omega_R}{2}(\hat{a}\hat{\sigma_+} + \hat{a}^\dagger\hat{\sigma_-}), \tag{31}$$

$$\Omega_R = (\frac{2d}{\hbar})\xi, \tag{32}$$

$$\xi = \sqrt{\frac{\hbar\omega}{2\varepsilon_\circ V}}. \tag{33}$$

Ω_R corresponds to the Rabi frequency which is proportional to the dipole moment d and ξ is the amplitude of an electric field in the mode volume V. $\hat{a}$ and $\hat{a}^\dagger$ are the creation and annihilation operators, respectively, that corresponds to the creation and destruction of photons and $\hat{\sigma_+}, \hat{\sigma_-}$ and $\hat{\sigma_z}$ are the Pauli matrices described in section 2.3.2. Let's introduce the detuning parameter δ measuring detuning of field mode frequency relative to electronic transition. In the basis $\binom{1}{0}=|e\rangle\,|0\rangle$ and $\binom{0}{1}=|g\rangle\,|1\rangle$, the Hamiltonian is

$$\hat{\mathrm{H}} = \frac{\hbar(\omega+\omega_o)}{2}\begin{pmatrix}1 & 0\\ 0 & 1\end{pmatrix} + \frac{1}{2}\begin{pmatrix}-\delta & -i\Omega_R\\ i\Omega_R & \delta\end{pmatrix}. \tag{34}$$

By diagonalizing the equation (34), we can obtain the following eigenvalues

$$E_\pm = \hbar\omega_\pm = \frac{\hbar(\omega+\omega_o)}{2} \pm \frac{1}{2}\sqrt{\delta^2+\Omega_R^2}. \tag{35}$$

We can define the generalized Rabi frequency of quantum model as $\Omega_g = \sqrt{\delta^2+\Omega_R^2}$. At resonance condition ($\delta = 0$) one gets the Rabi frequency $\Omega_g = \Omega$ and the system degeneracy of two energy states is lifted giving the energy separation by $\Delta E = \hbar\Omega_R$. The eigenstates of system that corresponds to eigen-values in equation (35) are called the dressed state which implies the naked states getting dressed by interaction with photons. Solving for the polaritonic eigenstates yields:

$$|P_+\rangle = \cos\theta\,|e\rangle\,|0\rangle + i\sin\theta\,|g\rangle\,|1\rangle\,, \tag{36}$$

$$|P_-\rangle = \sin\theta\,|e\rangle\,|0\rangle - i\cos\theta\,|g\rangle\,|1\rangle\,, \tag{37}$$

with angle θ defined by $\tan(2\theta) = -\frac{\Omega}{\delta}$. At resonance i.e. $\delta = 0$, one obtains two maximally entangled polaritonic states with angle $\theta = \pi/4$ as

$$|P_r-\rangle = \frac{1}{\sqrt{2}}(|e\rangle\,|0\rangle - i\,|g\rangle\,|1\rangle), \tag{38}$$

$$|P_r+\rangle = \frac{1}{\sqrt{2}}(|e\rangle\,|0\rangle + i\,|g\rangle\,|1\rangle). \tag{39}$$

The above eigenstates of the system implies the equal superposition of the ground state + one extra photon and excited state + zero or no extra photon. The half-matter half-light polaritons and Rabi splitting in shown in Figure 6.

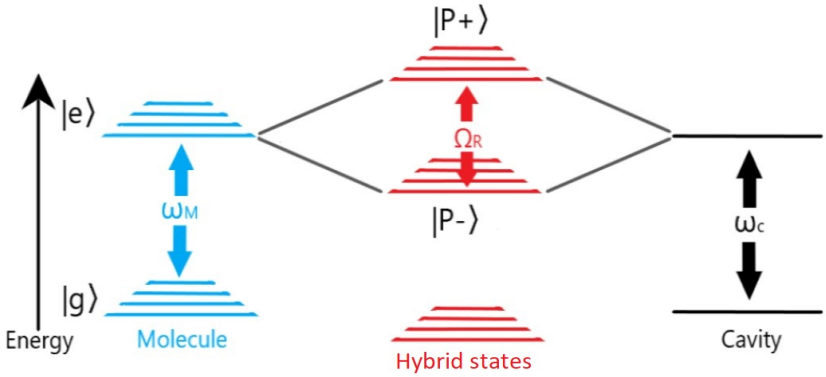

Figure 6. The coupled molecule and cavity system. Newly formed polariton states ($|P_-\rangle\,, |P_+\rangle$) are shown with Rabi splitting (Ω_R).

It should be noted here that the aforementioned results are in the limit of RWA which become invalid in ultrastrong coupling regime. In that case, one also needs to consider the anti-resonant part of Hamiltonian. The full Hamiltonian is given as

$$\hat{\mathrm{H}} = -\frac{1}{2}\hbar\omega_\circ\hat{\sigma_z} + \hbar\omega\hat{a}^\dagger\hat{a} - i\frac{\hbar\Omega_R}{2}(\hat{a} - \hat{a}^\dagger)(\hat{\sigma_+} + \hat{\sigma_-}). \tag{40}$$

Diagonalizing equation (40) will give us two more eigenstates i.e. new ground state of coupled system $|GS\rangle$ and the doubly excited state $|DE\rangle$.

2.3.4 Coupling multiple excitons

Finally, a many-body case is worth mentioning here due to its relevance with strong coupling with organic molecules. For a large number of molecules N, the system acts as a giant quantum oscillator extended to large number of molecules instead of one by using so-called Dicke or Tavis-Cummings Hamiltonian [35] given as

$$\hat{\mathrm{H}}_{\mathrm{TC}} \approx \hbar\omega_o(-\frac{N}{2} + \hat{b}^\dagger\hat{b}) + \hbar\omega\hat{a}^\dagger\hat{a} - i\frac{\sqrt{N}\hbar\Omega_R}{2}(\hat{a}^\dagger\hat{b} - \hat{b}^\dagger\hat{a}), \tag{41}$$

where $\hat{b}^{\dagger}$ and $\hat{b}$ are the new bosonic operators obtained from Holstein–Primakoff transformation. The main difference between Jaynes-Cummings and Tavis-Cummings Hamiltonian is that the first one considers only one coupled two state system while the other one treats molecular excitation as delocalized excitation and the excitation energy is shared among all N number of molecules with a total of N+1 states. Solving polaritonic eigenstates of $\hat{\mathrm{H}}_{\mathrm{TC}}$ leads us to Rabi splitting Ω_R

$$\hbar\Omega_R = 2\sqrt{N}d\xi. \tag{42}$$

The above equation implies that coupling strength can be increased by increasing the dipole moment of molecules, enhancing the electromagnetic field by confining it to smaller mode volume and by increasing the number of coupled molecules. The many-body system with N molecules also contain dark states in addition to the two bright polariton states. The term dark state is given as it can be constructed of pure molecular excitations or state that does not absorb or emit any photon thus not visible in spectroscopy as compared to the polaritonic states. The molecules in dark states are stable and posses non-zero energy thus they can act as a controlled energy reservoir from which energy can be extracted [36].

It is also worth mentioning here the possibility to strongly couple several different non-reactive active materials with the same cavity mode that give rise to hybrid microcavities. Such hybrid system requires the excitons of active materials to be of the same energy. In this scenario, one can obtain the hybridized polaritonic mode due to the mutual coupling of individual materials into the same light mode. These hybrid systems offers increased Rabi split than the individual systems as well as the room to engineer optoelectronic properties. For example, one can combine the tightly bound and stable Frenkel excitons to the unstable and delocalized Wannier-Mott excitons to obtain the Frenkel-Wannier-Mott cavities with hybrid properties [20, 21]. The hybrid cavities are expected to have long range energy transfer, shortening of relaxation times and short fluorescence decay times.

3 Materials and Methods

This chapter will provide thorough description of materials and methods used in our studies. In the first section, the structure and properties of 10-Hydroxybenzo[h]quinoline (HBQ) and Zinc Oxide (ZnO) will be discussed. The second section will elaborate the sample fabrication process followed by the last section in which the measurement setup will be discussed.

3.1 10-Hydroxybenzo[h]quinoline (HBQ)

The selection of molecule was the most important part of the strong coupling studies. In our research group's previous studies [37], Groenhof and Toppari used atomistic molecular dynamics simulation to simulate the ultrafast and directional proton transfer utilizing the strong coupling in 2-(2-hydroxyphenyl)benzothiazole (HBT) and Rhodamine (Rh) molecules. However, fabrication of this cavity was not realized due to practical limitations. Therefore, the structurally similar molecule i.e, HBQ was chosen to study the effect of strong coupling. It is extensively studied excited state intermolecular proton transfer molecular system [38] that has been verified experimentally [39]. The metal complexes of HBQ molecules are thermally stable and exhibit high Electroluminescence quantum efficiency, hence making them formidable candidate for organic optoelectronics devices [40]. The physical and chemical properties of HBQ is shown in Table 1 and the structure is shown in Figure 7.

Table 1. Physical and chemical properties of HBQ [41].

Molecular formula	$C_{13}H_9NO$
Molecular weight	195.22 g/mol
Appearance	Yellow crystalline
CAS	33155-90-7
Melting point	102-105^{o}C
Boiling point	420^{o}C
Density	1.307±0.06 g/cm^3

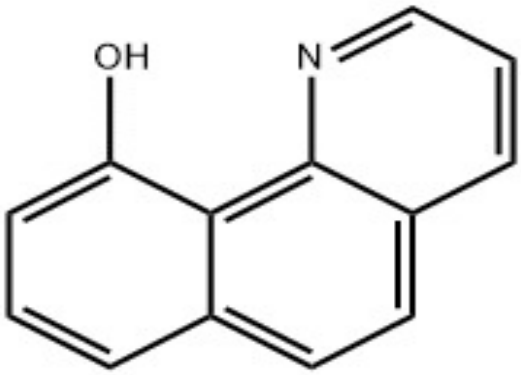

Figure 7. The structure of HBQ [41].

3.2 Zinc Oxide (ZnO)

The selection of suitable material to make hybrid cavities was second main task in this studies. After the careful analysis of wide range of materials, ZnO was considered to fabricate Hybrid HBQ-ZnO cavities. ZnO is a II-IV semiconductor that has a bang gap of 3.36 eV (370 nm). The thin films and nanoparticles of ZnO considered to be an excellent material for UV-Vis optoelectronics. Its large exciton oscillator strength can lead to large Rabi split and it has already been studied for strong coupling at room temperature [42, 43]. Due to its promising excitonic properties, it has also been theoretically proposed [44] and experimentally studied [45, 46] as an active material for polariton lasers. The general physical and chemical properties of ZnO is shown in Table 2 and the possible crystal structures are shown in Figure 8.

Table 2. Physical and chemical properties of ZnO [47]

Molecular formula	ZnO
Molecular weight	81.4 g/mol
Appearance	White powder
CAS	1314-13-2
Melting point	1974^oC
Refractive index	2.0041
Density	5.6 g/cm^3

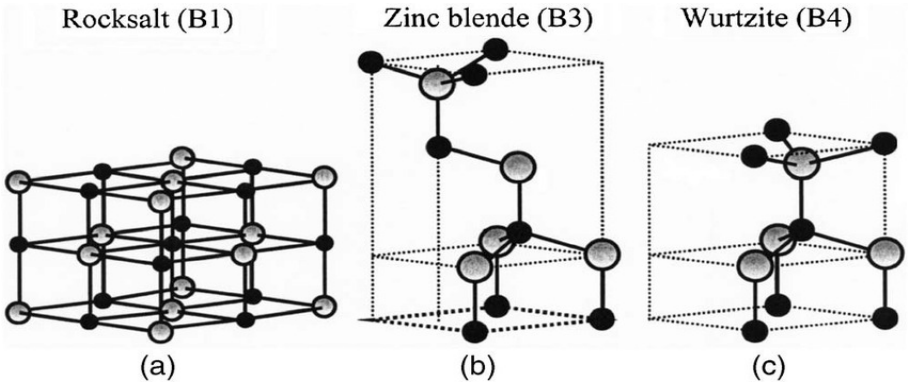

Figure 8. The possible crystal configuration of ZnO. (a) cubic rocksalt, (b) zinc blende and (c) hexagonal Wurtzite. The shaded gray and black spheres represent zinc and oxygen atoms, respectively. [48]

3.3 Sample Preparation

3.3.1 Cavity geometry

The precise geometry of Fabry-Pérot cavity is crucial to observe strong light-matter interaction. The cavity should confine light efficiently and cavity modes must be in resonance with molecular transitions to observe high coupling strength. The structure of the cavity is shown in Figure 9, where the active region is sandwiched between two aluminum mirrors. The top mirror thickness was set to 10 nm and 20 nm to study its effect on coupling energy. The films sample were fabricated in a similar fashion as shown in Figure 9 without the top aluminum mirror. The choice of mirror is crucial in the cavity geometry. For example, silver mirror has a better reflectivity, however, they leak around 370 nm due to its plasma frequency which is the absorption maximum of the materials used in this studies. Therefore, aluminum mirrors were chosen due to their tolerable reflectivity and faster deposition rate. Efficient confinement of light requires a high Q factor as well as the confined mode volume. Our research group already established asymmetric cavity designs with a thick bottom mirror and lossy top mirror keeping in mind that light should come out from either one of the mirrors to realize measurements [49]. TMM was utilized to optimize mirror thickness, which provides a satisfactory middle ground between Q factor, high enough confinement and top mirror transmittance [50]. After trying various geometries using TMM, top mirror thickness was settled on 20 nm or 10 nm and bottom mirror thickness to be 120 nm. The aluminum mirrors were evaporated

at the evaporation rate of 0.1 nm/s with an ultra-high vacuum e-beam evaporator (Instrumentti Mattila) which is the widely used technique to grow pure metal films.

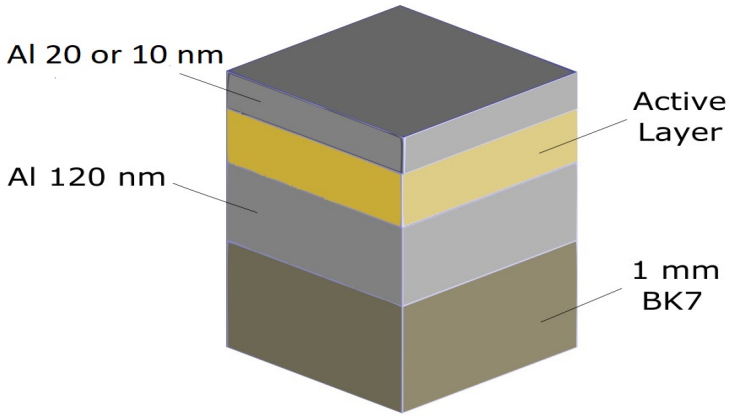

Figure 9. The illustration of cavity geometry. From top to bottom: 20 nm or 10 nm Al top mirror, 10-60 nm ZnO, 30-90 nm HBQ, ZnO+HBQ active layer, 120 nm Al bottom mirror, 1 mm BK7 substrate.

3.3.2 Substrate cleaning

All the samples were made on 15 mm×15 mm BK7 glass pieces. The glass pieces were first rinsed with deionized water and then high purity isopropanol. After rinsing, the glass pieces were submerged in isopropanol bath and left in the sonicator for 5 minutes. After sonication, they were rinsed again with isopropanol and blown dry with dry nitrogen.

3.3.3 HBQ spin solution preparation and thin film deposition

The choice of solvent and polymer matrix is very important in spin solution and consequently, the sample fabrication process. It should be chosen so that the solvent incorporate well with polymer matrix as well as the molecules. For this purpose, chlorobenzene was chosen as a solvent, and PMMA was chosen as the polymer matrix for HBQ molecules. PMMAC2 was purchased from (MicroChem) that contained 2% (mass percentage) PMMA and 98% chlorobenzene. The spin solution preparation was initiated by adding 16 mg of HBQ powder in 180 μl of chlorobenzene and vortexing it for 5 minutes to obtain 8% (Mass %) HBQ stock solution in chlorobenzene. After dissolving the HBQ, 1400 μl PMMAC2 and 980 μl chlorobenzene was added to the

stock solution and vortexed for 5 minutes to obtain 0.5 to 1 ratio of HBQ/PMMA solution.

The film thickness was calibrated each time as the HBQ molecules start agglomeration as well as evaporation during the sample baking, thus reduces the reproducibility. The calibration was carried out on bare BK7 glass pieces and the thin film was later spin-coated on actual samples after knowing the precise spin speed for the required thickness. For the calibration, glass pieces were cleaned carefully and 300 μl spin solution was spin-coated at different spin speeds. The films were then baked on a hot plate at 70 °C for 15 minutes. Then, the thickness was measured using a KLA Tencor P-15 profilometer from a scratch made onto the films using a sharp scalpel. The acquired data were plotted and fitted with linear or polynomial fit to determine the spin speed for required thickness. The obtained spin speed was then used to spin coat the spin solution on the bottom mirror evaporated glass piece. The description of HBQ cavities used in this thesis is given in Table 3.

Table 3. The description of HBQ cavities.

HBQ cavities			
Sample	HBQ:PMMA ratio	HBQ thin film thickness (nm)	Top mirror thickness (nm)
HBQ C1	0.5:1	100	20
HBQ C2	1:1	100	20
HBQ C3	1.6:1	100	20
HBQ C7	0.5:1	100	10

3.3.4 ZnO thin film deposition

The ZnO thin films were deposited using Beneq TFS 200 Atomic Layer Deposition (ALD) system. ALD is widely used technique for high quality thin film fabrication that provides atomic level precision. In the ALD process, the substrate is exposed sequentially to alternating precursors. The precursors reacts with surface of material in a self limiting way and layer by layer deposition is achieved by repeated exposure to the precursors. The most common recipe to grow ZnO uses diethylzinc (DEZ) and deionized water (H_2O) as a precursors and Nitrogen (N_2) as a purging gas. In our case, the recipe was already established in department of physics, JYU by Napari et al. [51].

The aluminum evaporated BK7 glass pieces were placed in the deposition chamber.

The deposition was carried out at 150°C using DEZ (95%, Strem Chemicals Inc., and electronic grade from SAFC Hitech) and deionized water as precursors and nitrogen as the carrier and purge gas. The reactor pressure was maintained at 5 mbars during the depositions. The deposition cycles were 0.3/10/0.3/10 s (DEZ/N2/H2O/N2). Long purge times ensured the efficient removal of the precursors and reaction by-products from the substrates. The growth studies found that 512 cycles corresponds to 100 nm ZnO thin film and number of cycles for required thickness were calculated keeping it as a reference.

3.3.5 Hybrid cavity fabrication

The total of four hybrid cavities were fabricated by varying the thickness of HBQ and ZnO thin films. The configurations were finalized by simulating the different cavity combinations on open source transfer matrix method based simulator known as filmetrics [50].

For the ZnO+HBQ hybrid cavities, ZnO was deposited on the bottom mirror. Meanwhile, ZnO deposited glass pieces were used for HBQ thickness calibration using the same protocol described in section 3.3.3. The ZnO glass pieces were used because the thickness of HBQ film deposited on top of the glass may vary from to the film on top of ZnO deposited samples. The ZnO deposited bottom mirror was later spincoated with HBQ and baked at 70°C for 15 minutes. After that, 20 nm or 10 nm top Al mirror was evaporated on the top of ZnO-HBQ thin films to obtain hybrid HBQ-ZnO cavity. The description of Hybrid cavities used in this thesis are given in Table 4.

Table 4. The description of HBQ-ZnO hybrid cavities.

Hybrid cavities			
Sample	ZnO thin film thickness (nm)	HBQ thin film thickness (nm)	Top mirror thickness (nm)
HBQ-ZnO C4	10	90	20
HBQ-ZnO C5	20	60	20
HBQ-ZnO C6	30	30	20
HBQ-ZnO C8	20	60	10
HBQ-Zn0 C9	30	30	10

3.4 Measurements

The measurements involved in this study include angle-resolved reflectance measurements. The reflectance measurement was performed at varying angles from 10° to 70° so that the reflectance dispersion could be measured. As described in section 3.3.1, the bottom mirror is non-transmitting (T=0), thus the absorption can be calculated from reflectance measurement using the following relation by putting the transmittance, T, to zero,

$$T + R + A = 1. \tag{43}$$

R corresponds reflection and A for absorption. When the molecular absorption and cavity modes are tuned, the symmetrical and equivalent polaritonic peaks appears on both sides of the molecular absorption energy. The separation between these two peaks gives the magnitude of Rabi split Ω_R energy given in equation (42).

3.4.1 Reflectance measurements

The deuterium lamp was used as the light source to excite the molecules inside the cavity. The lamp was turned on two hours before the measurements to have a stabilized lamp spectra. The lamp was kept in a separate box and light was directed from it to the sample through reflective silver mirrors acquired from Thorlabs. The light is passed through a polarizer followed by series of iris diaphragms to obtain a narrow enough and collimated beam to hit a sample within its dimensions. The sample was mounted on the sample holder with slight adjustability in x,y and z-direction, and the sample holder was fixed on the manually rotatable stage. The CCD camera was turned on 10 minutes before measurements to cool it down at -15°C. After both lamp and CCD stabilization, the lamp spectra were collected to be used in data analysis later.

The sample was aligned such that the beam hits the middle of the sample. In addition to this, it was made sure that the sample is not tilted and stands in the axis of rotation so that the reflected light beam is not clipped during the rotation. After the setup optimization and sample alignment, the reflectance measurement was taken from an incident angle of 10° to 70° with 5° increment. The reflected light was collected with a collimator objective attached to an optical fiber coupled to the spectrometer. The position of the detector needed to be adjusted for each angle, hence, it was mounted on the moving detector arm that was able to rotate

coaxially with the rotating stage. The spectra were recorded using a commercially available software (Andor technology) and then analyzed using Origin software. The schematic of the measurement setup is shown in Figure 10.

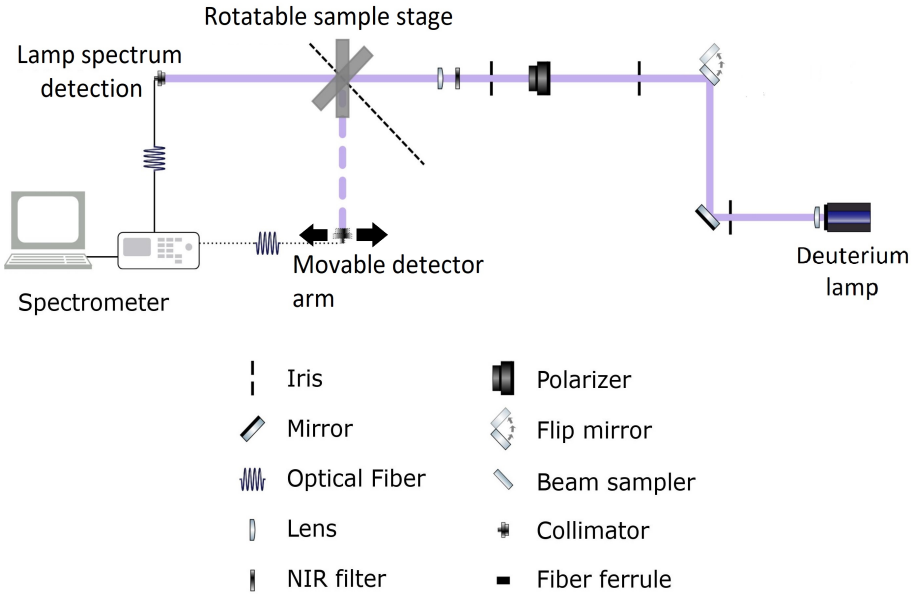

Figure 10. The measurement setup with components for reflectance measurement.

4 Results and Discussion

In this chapter, the experimentally obtained film absorption and cavity dispersion will be presented with 3D absorption and the contour plots. Firstly, the 10-Hydroxybenzo[h]quinoline (HBQ) molecule will be presented and the later part will be focused on HBQ and Zinc oxide (ZnO) hybrid cavities.

The dispersion of absorption was calculated for HBQ, ZnO, and HBQ-ZnO hybrid cavities. The reflection data was obtained from the reflection measurements explained in section 3.4.1. The obtained reflection data was then normalized by dividing it with lamp spectra to change the intensities from detector counts to relative intensities. Finally, the absorption was calculated with equation (43) by setting T=0.

The absorption data were fitted for each angle to extract the position of respective polaritons peaks. The fitting was performed by using Voigt and Asymmetric Double-Sigmoid (Asym2sig) profiles depending on the shape of peaks. Voigt is a peak function obtained as a convolution between the Cauchy-Lorentz and Gaussian line shapes with variable contribution of each, and Asym2sig is an asymmetric peak function that allows separate Gaussian linewidths for long and short wavelength sides. The baseline correction was needed due to unspecific random scattering from the top Al mirror showing as a non-even background feature within the obtained absorption spectra.

The resonant angles at which upper and lower polaritonic peaks are equal in height were estimated from the fittings of absorption plots while the Rabi split was calculated from the peak to peak distance at the resonant angle. The resonant angle of sample HBQ-ZnO C6 was not determined as upper polaritonic peaks were exceeding the energies of 3.8 eV which was out of the CCD detection limit.

There were also some uncertainties in the presented results that aroused from the multiple factors. The first factor was the instrumental limitation due to which the upper polariton branch was not observed in HBQ-ZnO C6. The second major factor was the peak position that was extracted through data fitting. The data fitting involved background correction with user-defined data points that could affect the sample analysis. Most of the time, the background was clearly detected and

removed, but in the samples with thinner top mirror (10 nm Al) this turned out to be problematic. Thus, inducing higher variation and possible higher error. The third uncertainty arises from the presence of middle polariton in the system. The middle polariton was observable at some angles, however, it was closely merged with the upper polariton branch. Therefore, the software could not distinguish the position and intensity of middle polariton reliably and it is not presented in the Figures 12, 13 and 14.

4.1 Films absorption

The 100 nm HBQ film, 55 nm ZnO film and 60 nm HBQ, 20 nm ZnO HBQ-ZnO film absorptions are presented in Figure 11. The film absorption was calculated by using Equation 43 and the absorption values were normalized to relative values. The absorption maxima of HBQ molecule is located at 375 nm and shoulder at 360 nm. The ZnO film and HBQ-ZnO hybrid film shows absorption maxima at 365 nm. It can also be seen in Figure 11 that the spectral shape of absorption and intensity has changed in HBQ-ZnO hybrid films.

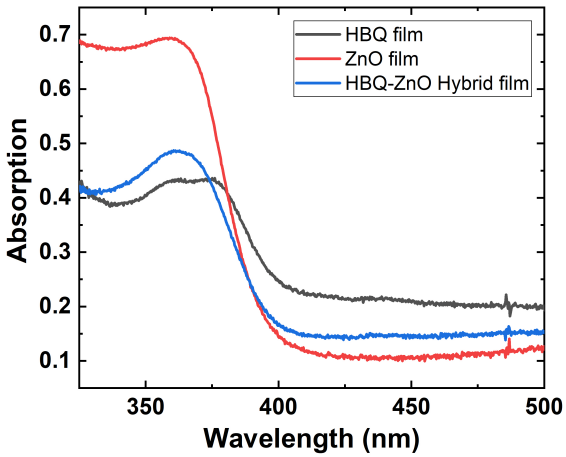

Figure 11. Absorption of HBQ (black), ZnO (red) and hybrid HBQ-ZnO (blue) thin films.

4.2 HBQ cavities

The 3D dispersion and contour plots of HBQ C1, HBQ C2 and HBQ C3 are presented in Figure 12. The blue highlighted peaks shows the resonant angle and Rabi splittings were calculated as 205 meV, 228 meV and 279 meV. The lowest concentration HBQ C1 cavity showed the Rabi split of 205 meV in Figures 12 (a, b) which was increased to 228 meV by increasing the concentration in the HBQ C2 cavity as shown in 12 (c, d). The highest Rabi split was observed in the highest concentration sample HBQ C3 as 228 meV demonstrated in 12 (e, f). Thus, increasing the concentration lead to the increased Rabi splittings as shown in equation (42). The further increase in the concentration lead to the agglomeration of HBQ molecules to form micron size structures that resulted in bad quality thin films and reproducibility of the samples.

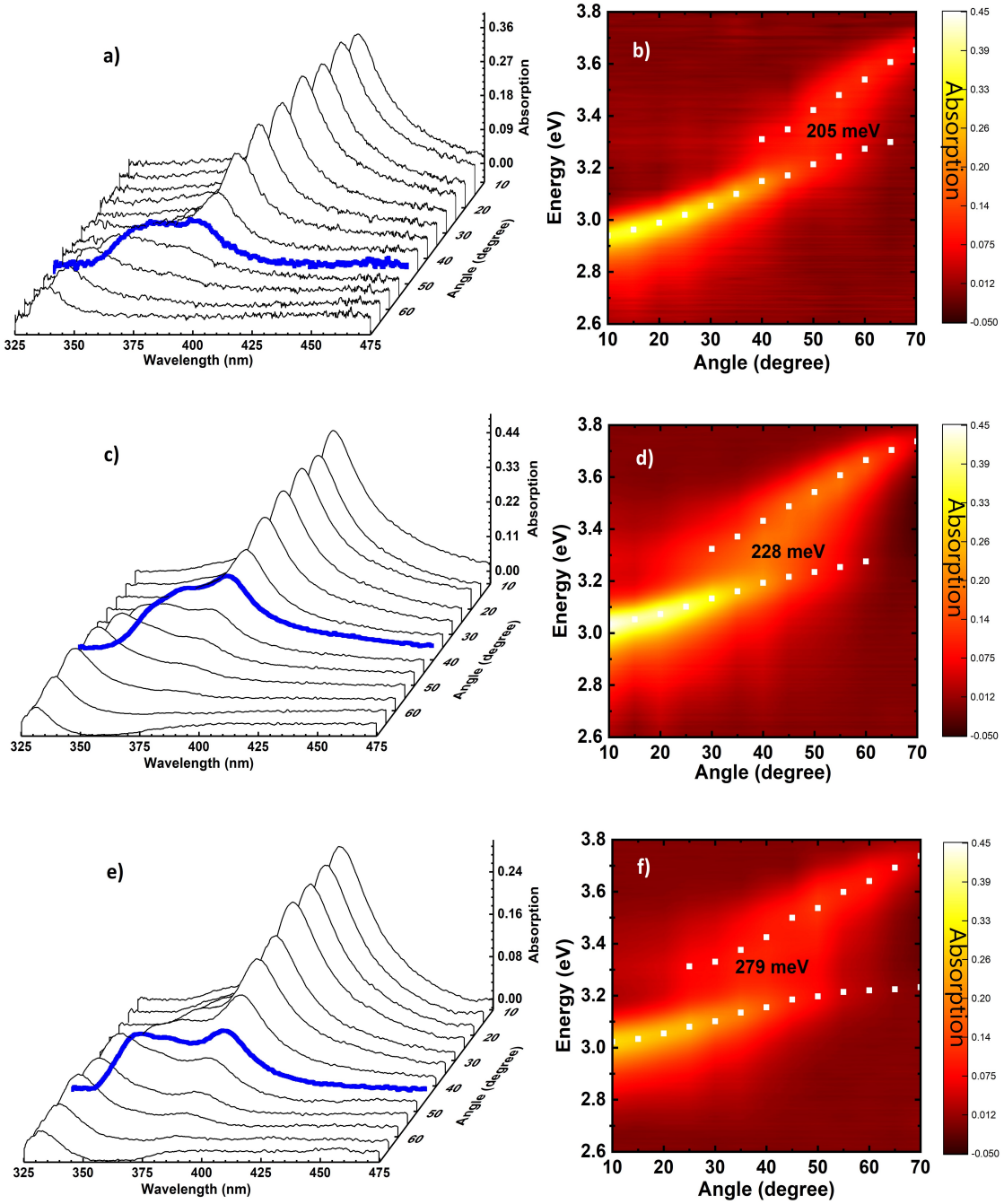

Figure 12. HBQ-cavity 3D dispersion plots with resonant angle absorption spectrum highlighted (blue) for (a) C1, (c) C2 and (e) C3. HBQ-cavity dispersions as contour plots with upper and lower polariton positions (white squares) for (b) C1, (d) C2 and (f) C3.

4.3 Hybrid cavities

The 3D dispersion and contour plots of hybrid HBQ-ZnO C4, HBQ-ZnO C5 and HBQ-ZnO C6 are presented in Figure 13. The increase of the ratio between PMMA and HBQ molecules in HBQ cavities led to the aggregation and poor fabrication reproducibility as described in previous section. This problem was addressed by fabricating hybrid cavities in which ZnO thin film was introduced in the system because it is chemical inactive with HBQ molecule and large oscillator strength that could lead to enhanced Rabi split. The hybrid cavities were made solely with the lowest concentration HBQ and ZnO thin films because lowest concentration HBQ cavities offers better fabrication reproducibility and more room for ZnO to increase the Rabi split. The Rabi splitting of 300 meV and 310 meV were observed in HBQ-ZnO C4 and HBQ-ZnO C5 as shown in Figures 13 (a, b, c and d), respectively, which was already more than the HBQ C1 cavity. The Rabi splitting of HBQ-ZnO C6 in 13 (e, f) could not be estimated because energies of the upper polariton branch were exceeding 3.8 eV. The increased Rabi splitting in the hybrid cavities demonstrates the possibility to couple two different systems with the single cavity mode and the total Rabi split in the case of hybrid cavities is the sum of Rabi splitting of different individual systems in the cavity. The broad distribution of higher and lower polariton branch indicates the presence of the middle polariton in the system. However, it is hard to extract with the data fitting.

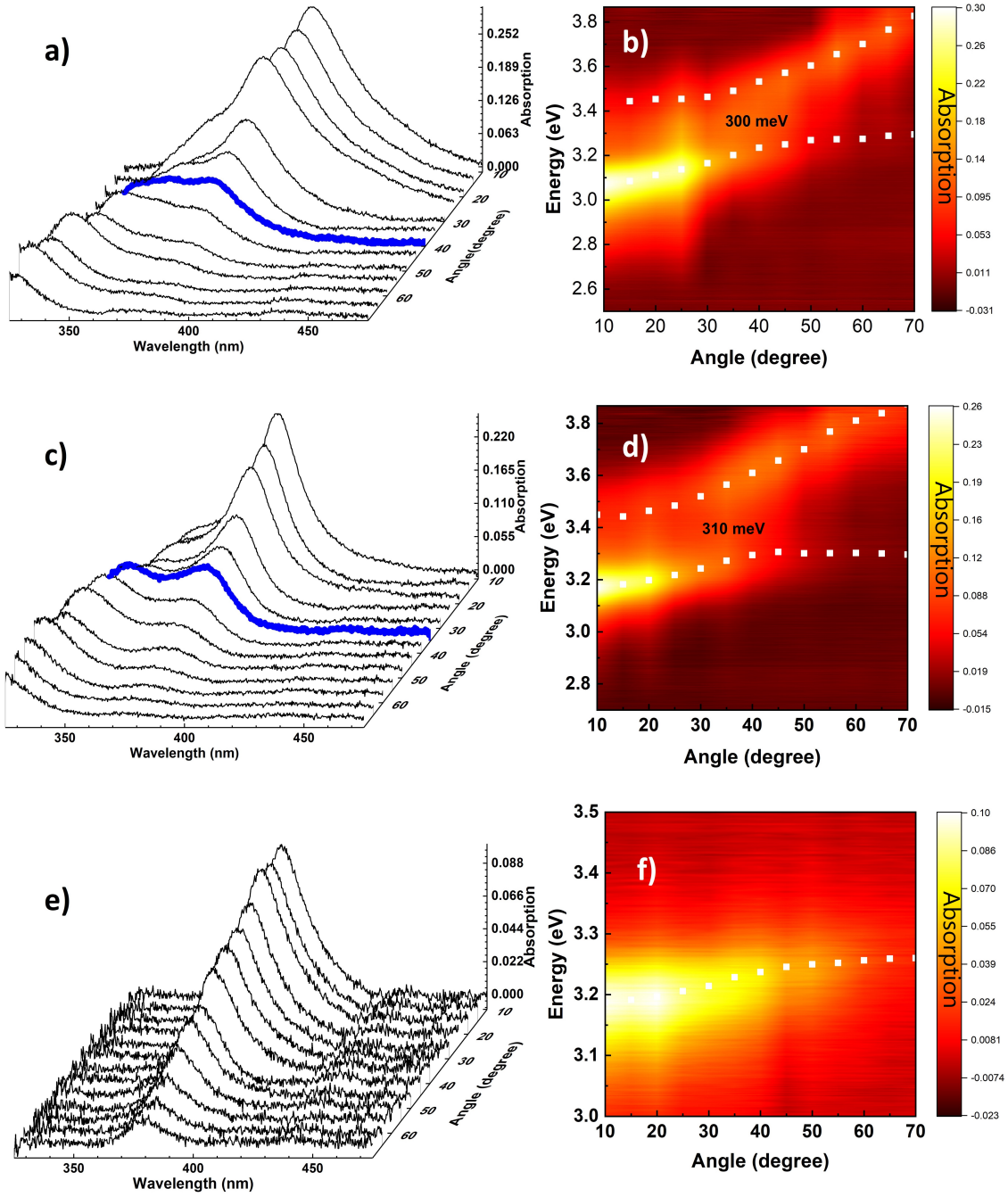

Figure 13. Hybrid-cavity 3D dispersion plots with resonant angle absorption spectrum highlighted (blue) for (a) C4, (c) C5 and (e) C6. Hybrid-cavity dispersions as contour plots with upper and lower polariton positions (white squares) for (b) C4, (d) C5 and (f) C6.

4.4 Cavities with 10 nm top mirror

The further increase in Rabi split was done by decreasing the top mirror thickness which was observed to be 380 meV, 430 meV, and 490 meV for HBQ-ZnO C7, HBQ-ZnO C8, and HBQ-ZnO C9 respectively. The decreased top mirror thickness will lead to increased cavity absorption due to less reflection from the top mirror. It can be seen in Figure 14, that the higher and lower polariton branch widens dramatically in case of these cavities and long tails can also be seen in the 3D dispersion plots which is the indication of increased absorption due to thin top mirror. Furthermore, the background was not anymore so reproducible which made the background correction hard because of above tails and absorption. This is visible as sudden jumps in the intensities between different angles in Figures. Furthermore, decreasing the top mirror thickness will also compromise the mode volume as well as the quality factor of the cavities to some extent.

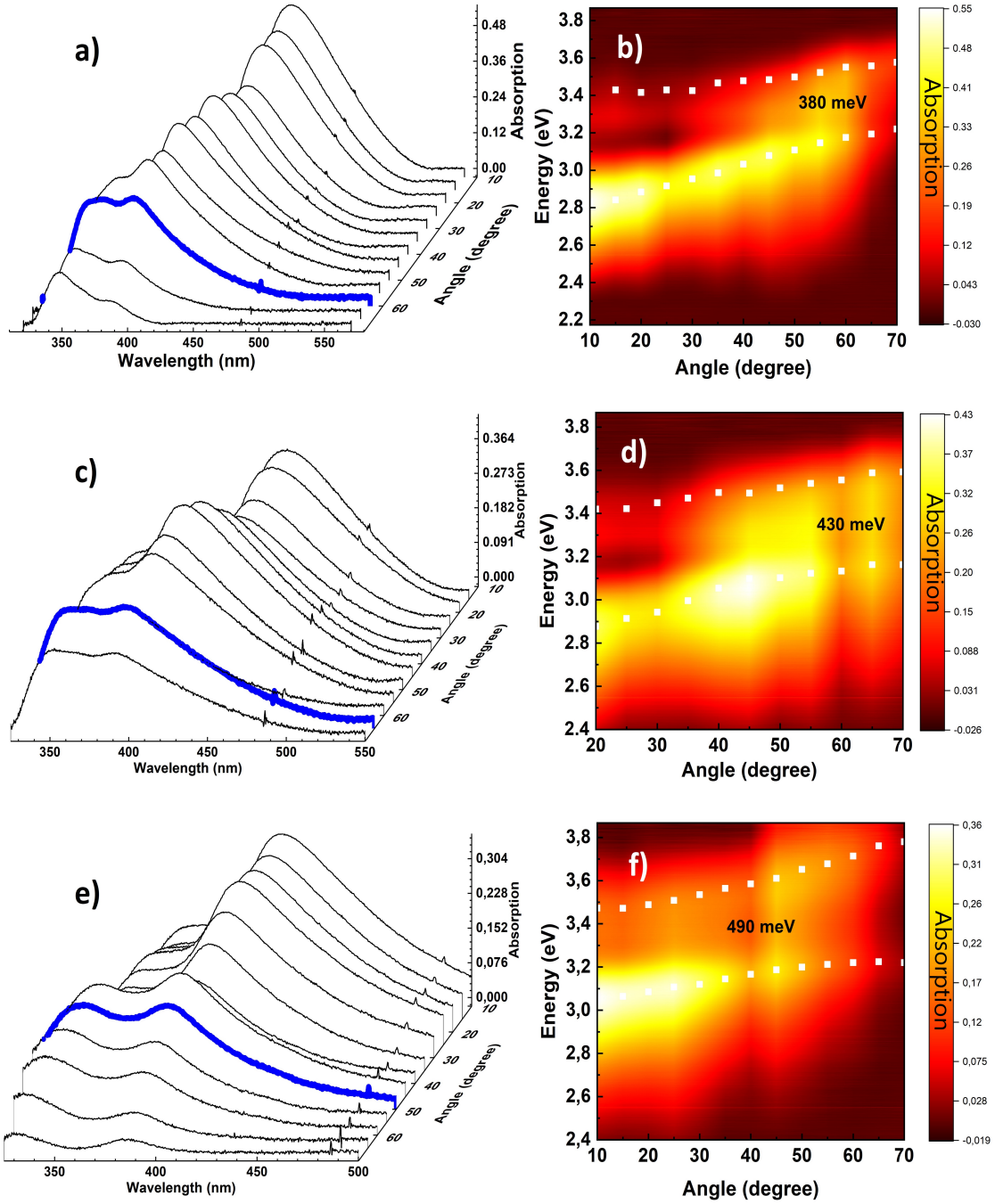

Figure 14. Hybrid-cavity with 10 nm top mirror 3D dispersion plots with resonant angle absorption spectrum highlighted (blue) for (a) C7, (c) C8 and (e) C9. Hybrid-cavity with 10 nm top mirror dispersions as contour plots with upper and lower polariton positions (white squares) for (b) C7, (d) C8 and (f) C9.

5 Conclusions

To conclude the main results of the thesis, various strongly coupled systems were studied over the range of Rabi split energies. The studied system for this thesis were HBQ microcavities and hybrid HBQ-ZnO microcavities. The suitable cavity combination was acquired by using the TMM. The HBQ cavities showed the minimum Rabi split of 205 meV for 0.5:1 HBQ to PMMA ratio and a maximum of 228 meV for 1.6:1 HBQ to PMMA ratio which testifies the equation (42) that increase in concentration leads to the increase in Rabi splittings. The further increase in the HBQ to PMMA concentration leads to the aggregation of HBQ molecules, substandard thin films and poor experimental reproducibility of the samples. Therefore, an alternative approach was needed to enhance the Rabi split. This was addressed by fabricating hybrid cavities by introducing ZnO thin film in the cavities. The ZnO was chosen for its chemical un-reactiveness with HBQ molecule and large oscillator strength. The ZnO thin films were only introduced to the lowest concentration HBQ sample to obtain the enhanced Rabi split of 310 meV. The further enhancement was realized by compromising the quality factor by decreasing the top mirror thickness to achieve the coupling energy of as much as 490 meV. The increased coupling energy confirmed the possibility to couple multiple materials with the single cavity mode as predicted theoretically by Agranovich et al. in 1997 [18].

In general, the overall aim of the thesis was to experimentally observe and develop an understanding of the strong coupling phenomena by using hybrid cavities. However, the main aim of this project is to investigate the effect of increased strong coupling on dark states and consequently, fluorescence yield of the molecule. The acquired knowledge from the thesis can be implemented to investigate the nature of dark states, fluorescence yield as well as the change in the chemical environment of the molecules for the polariton chemistry applications. The future proceedings on the current studies could be the detailed excitation and emission studies on HBQ and HBQ-ZnO hybrid cavities to get the detailed analysis on fluorescence yield of the system and to investigate the trend in fluorescence yield with progression in strong coupling.

References

[1] J. A. Hutchison et al. “Modifying Chemical Landscapes by Coupling to Vacuum Fields”. In: *Angewandte Chemie International Edition* 51.7 (2012), pp. 1592–1596. DOI: 10.1002/anie.201107033.

[2] P. Törmä and W.L. Barnes. “Strong coupling between surface plasmon polaritons and emitters: a review”. In: *Reports on Progress in Physics* 78.1 (2015), pp. 1–34. DOI: 10.1088/0034-4885/78/1/013901.

[3] E.M Purcell. “Proceedings of the American Physical Society”. In: *Phys. Rev.* 69 (11-12 June 1946), pp. 674–674. DOI: 10.1103/PhysRev.69.674.2.

[4] W.T. Simpson and D.L. Peterson. “Coupling Strength for Resonance Force Transfer of Electronic Energy in Van der Waals Solids”. In: *The Journal of Chemical Physics* 26.3 (1957), pp. 588–593. DOI: 10.1063/1.1743351.

[5] M. Ashraf M. Kasha H. R. Rawls. “The exciton model in molecular spectroscopy”. In: *Pure and Applied Chemistry* 11.3-4 (1965), pp. 371–392. DOI: 10.1351/pac196511030371.

[6] J.B. Khurgin. “Excitonic radius in the cavity polariton in the regime of very strong coupling”. In: *Solid State Communications* 117.5 (2001), pp. 307–310. DOI: 10.1016/S0038-1098(00)00469-5.

[7] C. Ciuti, G. Bastard, and I. Carusotto. “Quantum vacuum properties of the intersubband cavity polariton field”. In: *Phys. Rev. B* 72 (11 Sept. 2005), p. 115303. DOI: 10.1103/PhysRevB.72.115303.

[8] A. Auer and G. Burkard. “Entangled photons from the polariton vacuum in a switchable optical cavity”. In: *Phys. Rev. B* 85 (23 June 2012), p. 235140. DOI: 10.1103/PhysRevB.85.235140.

[9] C. Emary and T. Brandes. “Chaos and the quantum phase transition in the Dicke model”. In: *Phys. Rev. E* 67 (6 June 2003), p. 066203. DOI: 10.1103/PhysRevE.67.066203.

[10] García R. et al. “Circuit quantum electrodynamics in the ultrastrong-coupling regime”. In: *Nature Physics* 776 (2010), pp. 772–776.

[11] Y. Todorov et al. “Ultrastrong Light-Matter Coupling Regime with Polariton Dots”. In: *Phys. Rev. Lett.* 105 (19 Nov. 2010), p. 196402. DOI: 10.1103/PhysRevLett.105.196402.

[12] J. Casanova et al. “Deep Strong Coupling Regime of the Jaynes-Cummings Model”. In: *Phys. Rev. Lett.* 105 (26 Dec. 2010), p. 263603. DOI: 10.1103/PhysRevLett.105.263603.

[13] J. J. Hopfield. “Theory of the Contribution of Excitons to the Complex Dielectric Constant of Crystals”. In: *Phys. Rev.* 112 (5 Dec. 1958), pp. 1555–1567. DOI: 10.1103/PhysRev.112.1555.

[14] E. T. Jaynes and F. W. Cummings. “Comparison of quantum and semiclassical radiation theories with application to the beam maser”. In: *Proceedings of the IEEE* 51.1 (Jan. 1963), pp. 89–109. DOI: 10.1109/PROC.1963.1664.

[15] G.N.Zhizhin V.A.Yakovlev V.G.Nazin. “The surface polariton splitting due to thin surface film LO vibrations”. In: *Optics Communications* 15.2 (1975), pp. 293–295. DOI: 10.1016/0030-4018(75)90306-5.

[16] D. Meschede, H. Walther, and G. Müller. “One-Atom Maser”. In: *Phys. Rev. Lett.* 54 (6 Feb. 1985), pp. 551–554. DOI: 10.1103/PhysRevLett.54.551.

[17] C. Weisbuch et al. “Observation of the coupled exciton-photon mode splitting in a semiconductor quantum microcavity”. In: *Phys. Rev. Lett.* 69 (23 Dec. 1992), pp. 3314–3317. DOI: 10.1103/PhysRevLett.69.3314.

[18] V. Agranovich, H. Benisty, and C. Weisbuch. “Organic and inorganic quantum wells in a microcavity: Frenkel-Wannier-Mott excitons hybridization and energy transformation”. In: *Solid State Communications* 102.8 (1997), pp. 631–636. DOI: 10.1016/S0038-1098(96)00433-4.

[19] Lidzey D.G. et al. “Strong exciton-photon coupling in an organic semiconductor microcavity”. In: *Nature* 395.6697 (Sept. 1998), pp. 53–55. DOI: 10.1038/25692.

[20] D.G. Lidzey et al. “Hybrid polaritons in strongly coupled microcavities: experiments and models”. In: *Journal of Luminescence* 110.4 (2004). 325th Wilhelm and Else Heraeus Workshop. Organic Molecular Solids : Excited Electronic States and Optical Properties, pp. 347–353. DOI: 10.1016/j.jlumin.2004.08.031.

[21] M. Slootsky et al. “Room Temperature Frenkel-Wannier-Mott Hybridization of Degenerate Excitons in a Strongly Coupled Microcavity”. In: *Phys. Rev. Lett.* 112 (7 Feb. 2014), p. 076401. DOI: 10.1103/PhysRevLett.112.076401.

[22] A. Einstein. “Über einen die Erzeugung und Verwandlung des Lichtes betreffenden heuristischen Gesichtspunkt”. In: *Annalen der Physik* 322.6 (1905), pp. 132–148. DOI: https://doi.org/10.1002/andp.19053220607.

[23] P. Atkins, J. Paula, and R. Friedman. *Quanta, matter, and change: a molecular approach to physical change*. International series of monographs on physics. (W. H. Freeman, 2008.

[24] J. Peatross and M. Ware. “Physics of Light and Optics: A Free Online Textbook”. In: *Frontiers in Optics 2010/Laser Science XXVI*. Optical Society of America, 2010, JWA64.

[25] B. Harbecke. “Coherent and incoherent reflection and transmission of multilayer structures”. In: *Applied Physics B* 39.3 (Mar. 1986), pp. 165–170. DOI: 10.1007/BF00697414.

[26] F. Li. “Fabrication and characterization of ZnO-based microcavities working in the strong coupling regime : polariton laser”. In: 2013.

[27] B. Saleh and M.C. Teich. *Fundamentals of Photonics*. pure and applied optics. Wiley-Interscience, 2007. ISBN: 0471358320.

[28] M. Barth et al. “Nanoassembled Plasmonic-Photonic Hybrid Cavity for Tailored Light-Matter Coupling”. In: *Nano Letters* 10.3 (2010), pp. 891–895. DOI: 10.1021/nl903555u.

[29] K. Srinavasan et al. “Cavity Q, mode volume, and lasing threshold in small diameter AlGaAs microdisks with embedded quantum dots”. In: *Opt. Express* 14.3 (Feb. 2006), pp. 1094–1105. DOI: 10.1364/OE.14.001094.

[30] L. Novotny. “Strong coupling, energy splitting, and level crossings: A classical perspective”. In: *American Journal of Physics* 78.11 (2010), pp. 1199–1202. DOI: 10.1119/1.3471177.

[31] J. Halas et al. “Plasmons in Strongly Coupled Metallic Nanostructures”. In: *Chemical Reviews* 111.6 (2011), pp. 3913–3961. DOI: 10.1021/cr200061k.

[32] Gilbert G. *Introduction to Quantum Optics From the Semi-classical Approach to Quantized Light*. Oxford Master Series in Physics. CAMBRIDGE UNIVERSITY PRESS, 2010. ISBN: 978-0-521-55112-0.

[33] A. Delga et al. “Quantum Emitters Near a Metal Nanoparticle: Strong Coupling and Quenching”. In: *Phys. Rev. Lett.* 112 (25 June 2014), p. 253601. DOI: 10.1103/PhysRevLett.112.253601.

[34] M. Cirio et al. “Ground State Electroluminescence”. In: *Phys. Rev. Lett.* 116 (11 Mar. 2016), p. 113601. DOI: 10.1103/PhysRevLett.116.113601.

[35] V.V. Dodonov and V.I. Man’ko. *Theory of Nonclassical States of Light*. CRC Series in Pure and Applied Physics. CRC Press, 2003. ISBN: 9780367395353.

[36] Y.I. Ozhigov. *Space of dark states in Tavis-Cummings model*. 2019. arXiv: 1606.08483 [quant-ph].

[37] G. Groenhof and J.J. Toppari. “Coherent Light Harvesting through Strong Coupling to Confined Light”. In: *The journal of physical chemistry letters* 9.17 (Sept. 2018), pp. 4848–4851. DOI: 10.1021/acs.jpclett.8b02032.

[38] S. Hristova et al. “10-Hydroxybenzo[h]quinoline: switching between single- and double-well proton transfer through structural modifications”. In: *RSC Adv.* 5 (124 2015), pp. 102495–102507. DOI: 10.1039/C5RA20057A.

[39] C. Schriver et al. “The interplay of skeletal deformations and ultrafast excited-state intramolecular proton transfer: Experimental and theoretical investigation of 10-hydroxybenzo[h]quinoline”. In: *Chemical Physics* 347.1 (2008), pp. 446–461. DOI: 10.1016/j.chemphys.2007.10.021.

[40] H.P Shi et al. “Theoretical studies on structures and spectroscopic properties of 10-hydroxybenzo[h]quinoline zinc(II) and its derivatives substituted by cyano-groups”. In: *Journal of Molecular Structure: THEOCHEM* 950.1 (2010), pp. 53–63. DOI: 10.1016/j.theochem.2010.03.037.

[41] *Compound Summary for CID 11816407, 10-Hydroxybenzo[h]quinoline*. Open source. publisher: PubChem. May 2021. URL: https://pubchem.ncbi.nlm.nih.gov/compound/10-Hydroxybenzo_h_quinoline..

[42] J.R. Chen et al. "Large vacuum Rabi splitting in ZnO-based hybrid microcavities observed at room temperature". In: *Applied Physics Letters* 94 (Feb. 2009), pp. 061103–061103. DOI: 10.1063/1.3079398.

[43] R. Shimada et al. "Cavity polaritons in ZnO-based hybrid microcavities". In: *Applied Physics Letters* 92.1 (2008), p. 011127. DOI: 10.1063/1.2830022.

[44] R. Johne, D. D. Solnyshkov, and G. Malpuech. "Theory of exciton-polariton lasing at room temperature in ZnO microcavities". In: *Applied Physics Letters* 93.21 (2008), p. 211105. DOI: 10.1063/1.3036895.

[45] T. Guillet et al. "Polariton lasing in a hybrid bulk ZnO microcavity". In: *Applied Physics Letters* 99 (2011), pp. -. DOI: 10.1063/1.3650268.

[46] Helena F. et al. "Ballistic propagation of exciton–polariton condensates in a ZnO-based microcavity". In: *New Journal of Physics* 14.1 (Jan. 2012), p. 013037. DOI: 10.1088/1367-2630/14/1/013037.

[47] *Zinc oxide*. Open source. May 2021. URL: https://pubchem.ncbi.nlm.nih.gov/compound/Zinc-oxide#section=CAS.

[48] Ü. Özgür et al. "A Comprehensive Review of ZnO Materials and Devices". In: *Journal of Applied Physics* 98 (Aug. 2005), pp. 041301–041301. DOI: 10.1063/1.1992666.

[49] Arpan D., Ville T., and J. J. Toppari. "Optimizing geometry of low-Q all-metal Fabry-Pérot microcavity for fluorescence spectroscopy". In: *IOP SciNotes* 2.1 (Mar. 2021), p. 015205. DOI: 10.1088/2633-1357/abec2b.

[50] *Spectral Reflectance Calculator for Thin-Film Stacks*. URL: https://www.filmetrics.com/reflectance-calculator (visited on 07/10/2021).

[51] Mari N. et al. "Room-temperature plasma-enhanced atomic layer deposition of ZnO: Film growth dependence on the PEALD reactor configuration". In: *Surface and Coatings Technology* 326 (2017), pp. 281–290. DOI: 10.1016/j.surfcoat.2017.07.056.